Migration Letters

Volume: 21, No: S6 (2024), pp. 59-75

ISSN: 1741-8984 (Print) ISSN: 1741-8992 (Online)

www.migrationletters.com

Solar Cells Sensitized With Zinc Oxide Dye Modified With Aluminium Oxide

Eduardo Palacios Loayza[1] , Russell Nazario Ticse[2] , María Quintana Cáceda[3]

Abstract

In this paper, solar cells with ZnO electrode modified with Al2O3, were manufactured and characterized, through the sol gel process: the precursor used was Zinc Nitrate hexahydrate (Zn (NO3)2.6H2O) [0.1 M] and triethalonamine (TEA) [0.1M] was added with a heat treatment (100 °C) and later by precipitation, the ZnO nanoparticles were obtained. They were then sensitized with the N719. The paste used to obtain the ZnO film is modified with Al2O3 in different percentages. This modification is achieved when the precursor (Al (NO3)3.9H2O) is added to the aqueous suspension of ZnO. For this procedure the following characterizations were made: (1) XRD to check the crystal lattice of ZnO; (2) SEM to observe the rod-like morphology of the sample and with an average grain size of 90 nm, the nanoporosity of the samples was also observed; (3) UV Vis to check the absorption spectrum of the dye that is in the visible region; (4) EDS to check the presence of Aluminium and Zinc, (5) IV to determine the efficiency of the cell (0.39%); (6) OCVD to determine electron life time as a function of voltage; (7) IPCE to measure quantum efficiency (maximum 13%); (8) FTIR to identify and verify the existence of functional groups in the cell; (9) EIS that allows the determination of the parameters: electron half-life, electron transport time, resistance of the ZnO/dye/electrolyte interface, resistance of the film capacitive behaviour of the cell, which are important data that allow knowing the chemical and electrochemical processes of the cells.

Keywords: *solar cell, zinc oxide, modified electrode, sensitized, aluminium oxide.*

Introduction.

Richard E. Smalley, 1996 Nobel laureate in chemistry wrote an article [1], where he listed the top ten majo[1]r problems humanity will face in the next fifty years: energy

[1]Centro de Desarrollo de Materiales Avanzados y Nanotecnología, Universidad Nacional de Ingeniería, Lima, Perú, ORCID: 0000-0002-0647-7577
[2]Universidad Autónoma del Perú, Lima - Perú, ORCID: 0000-0002-6224-0830
[3]Centro de Desarrollo de Materiales Avanzados y Nanotecnología, Universidad Nacional de Ingeniería, Lima, Perú, Scopus Author Identifier: 57201765638

shortage; scarcity of drinking water; food shortage; environmental degradation; extreme poverty; terrorism and wars; diseases; access to education; dictatorship and increase in world population [2],[3]. Energy is in first place, but solving it implies development and economic prosperity, but it also damages the environment and therefore human health. In this scenario, the challenge is to generate it, but in a clean and cheap way, so that everyone has access to it. The second problem on the list is water scarcity. Millions of people live on our planet without access to drinking water. Given the increase in population and the depletion of aquifer reserves, it is necessary to find new sources of clean water. Luckily our planet has great water resources, but it contains salt and is located far away from where it is needed. In view of this, the problem can be solved by desalinating the water and pumping it long distances, but it must be done with low-cost energy; otherwise we will not solve the water shortage. The third problem of food scarcity is also solved with energy to harvest crops and distribute food using low-cost energy as much as possible to eradicate hunger and extreme poverty. The fourth problem is solved by minimizing the impact on the environment through clean energy consumption policies and drastically reducing the consumption of fossil fuels. The fifth problem of poverty is alleviated with low-cost energy. It can be pointed out that energy is the solution to most of the problems that afflict humanity.

By 2050 the world population will be approximately ten billion people [4], and according to energy experts, they predict that our planet would need 30 TW of energy resources for that year to maintain economic growth [5] and in an optimal projection every one of the inhabitants must have access to clean and cheap energy. Faced with this situation, renewable energies will play an important role in meeting energy needs as a clean alternative, photovoltaic solar cells being one of the best alternatives.

Solar cells provide clean energy because solar energy is converted directly into electrical energy without emitting carbon dioxide. Solar energy has no limits, it is free and it is distributed evenly to all human beings. Crystalline silicon solar cells have been extensively studied and are used in a number of applications due to their enormous advantages over other forms of energy, since these devices have no transmission losses, operate without noise, and require little maintenance. However, the excessive cost and the enormous energy required for its manufacture have caused a high price that prevents its mass use in the generation of photovoltaic energy. For this reason, its application is limited despite its considerable development in the last three decades [6].

ORCID : 0000-0002-2677-6179

In this perspective, dye-sensitized solar cells (DSCC) are promising mainly due to their low cost and easy fabrication. For this reason, many investigations are carried out to improve its performance and efficiency [7], maintaining low-cost [8], such as: using chemical methods (Sol-Gel) [3],[9], to find electrodes [3],[10], finding new dyes [11], evaluation of blocking layers [12]. The objective of this research is to manufacture and characterize solar cells with a ZnO electrode modified with Al2O3, the doping of the electrode modifies the energy level of the electrode, modifying the performance of the solar cell.

Experimental

Sol-Gel process

ZnO nanoparticles were obtained using the sol gel process [9]. For the synthesis of ZnO, an aqueous solution of Zinc nitrate hexahydrate (Zn(NO3)2.6H2O) at 0.1M and TEA (triethanolamine: C6H15NO3) at 0.1M was used. The solution was poured into a closed glass bottle and taken to a thermal process at 100 °C for 24 h, then it is decanted and washed with distilled water [13]. To obtain the ZnO powder, a heat treatment was carried out again for 8 h at 60 °C. The final paste was obtained by combining 1 g of ZnO for every 2 g of water. 2.2.

Electrode Preparation

Al2O3 modified ZnO nanostructured films were prepared by the following method. In an aqueous solution of ZnO, previously produced and explained in the previous paragraph, different amounts of Al (NO3)3.9H2O are added in order to obtain different amounts of Al2O3 in the final film. It has been proposed that the weight percentages of Al2O3 with respect to ZnO vary between 1 and 3%. Pure ZnO films have also been prepared for use as a reference. The suspension was magnetically stirred for 24 h and then deposited by doctor's blading method on a conductive substrate (SnO2:F) in a 0.25 cm2 square area formed by magic tape. It was left to dry at room temperature for 2 h and then the working electrode was heat treated at 380 °C for 45 minutes [12].

Solar cell preparation

The electrodes were sensitized with dye by immersing the substrate with the deposited film for 15 h in a container with dye N719 (cis-diisothiocyanato-bis (2,2'-bipyridyl-4,4'-dicarboxylate) ruthenium (II) bis (tetrabutylammonium)) to 0.5mM. Excess dye on the electrode surface was removed with ethanol. On the other hand, the counter electrode is covered with a platinum film by applying a drop of a 5mM H2PtCl6 (chloroplatinic acid) solution on a conductive substrate and a heat treatment of 450 °C for 15 minutes [12].

Solar cell assembly

Once the working electrode sensitized with N719 and the platinized counter electrode are ready, we proceed to seal the cell, which consists of placing the surlyn on the electrode as a frame in such a way that it does not cover the area of the ZnO film and that allows the injection of the electrolyte. Subsequently, by means of a thermal procedure (120°C) the surlyn melts and in this way the cell is sealed. Then the silver paint is placed on the inner edges of the counter electrode and the electrode, using a pipette we proceed to add one or two drops of the iodide/triiodide electrolyte through the side openings as shown in Figure 1 to introduce the electrolyte to the film of ZnO [11].

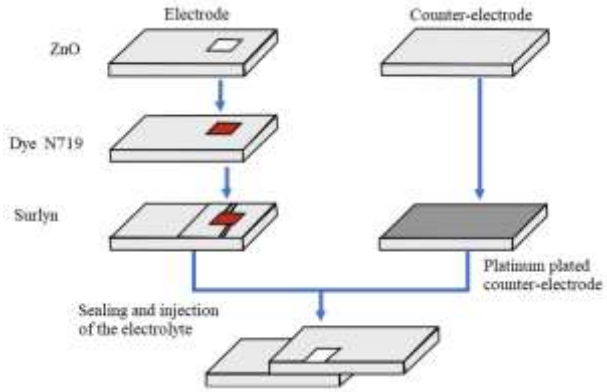

Fig 1 Assembly of the ZnO solar cell sensitized with N719.

Results

X-ray diffraction (XRD)

Figure 2 shows the diffractogram of the sample and the characteristic peaks of wurtzite-type ZnO can be clearly seen (standard pattern in JCPDS card number 36-1451), as well as the peaks of the conductive film of the substrate (SnO_2: F).

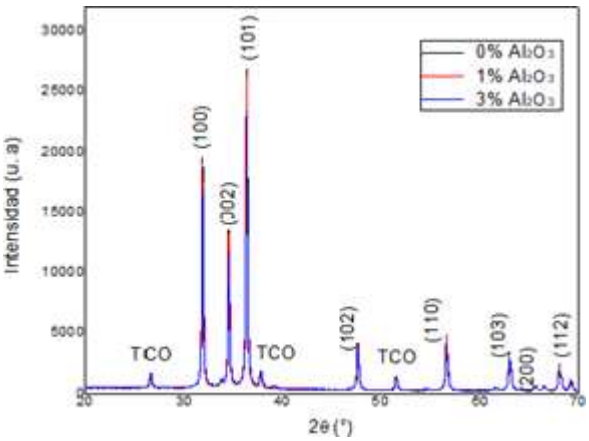

Fig 2. X-ray diffractogram of ZnO modified with various percentages of Al_2O_3.

Determination of crystallite size.

When the x-ray beam falls on the crystal, a portion is reflected by the planes of the crystal towards the detector to form the diffraction pattern; however, when the planes of the crystal contract, the rays are deflected from their original position, which produces a change in the diffraction pattern. When a defect occurs in the same crystal, x-rays are diffracted at various angles from each plane and cause a broadening of the diffraction pattern peaks. Other crystal defects also influence peak broadening, such as: crystallite size, sample inhomogeneity, microstrain which depends on non-uniform lattice distortions, faults and dislocations [14]. However, the peak broadening is not only due to the sample, it is also due to the instrument. Ideally, the peak should behave like a delta(δ) function with negligible width. A careful observation of the pattern shows us that there is a doublet in the characteristic peaks (Kα1 and Kα2), the ratio of intensities from the first to the second is approximately 2 to 1 [15]. To calculate the exact parameters of the diffraction pattern, only

Kα1 will be taken into account and for this, the composite peak must be deconvoluted in two, as shown in figure 3.

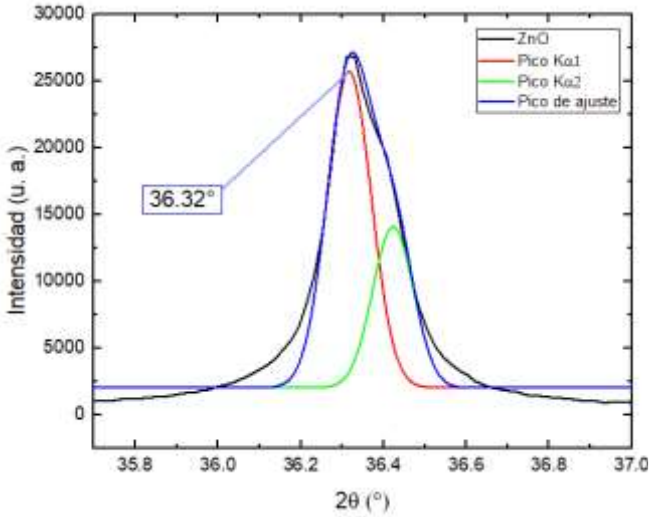

Fig. 3 Deconvolution of the ZnO diffraction pattern peak.

Table 1. Parameters obtained in the diffractogram with the origin program (where d is the size of the crystallite; ∈ is the microtension and δ is the dislocation)

(hkl)	2θ (°) JCPDS 036 145	2θ (°) Sample	β (°)	D (nm)	ϵ (10^{-3})	δ(nm^{-2})
100	31,770	31,832	0,133	64,169	2,0350	0,00023
200	34,442	34,490	0,135	64,169	1,9031	0,00024
101	36,353	36,320	0,142	61,439	1,8906	0,00026
102	47,539	47,605	0,159	57,043	1,5725	0,00030
110	56,603	56,653	0,175	53,755	1,4193	0,00034
103	62,864	62,922	0,185	52,147	1,3218	0,00036
200	66,379	66,438	0,192	51,654	1,2793	0,00037
112	67,961	68,007	0,181	55,199	1,1727	0,00032
201	69,100	69,149	0,176	57,075	1,1177	0,00030

From the table it can be seen that the positions of the peaks taken from the diffraction pattern of the ZnO sample, compared to the standard pattern, are slightly displaced towards positions of greater angles and therefore the type of microtension can be identified, which is tensile microstress [16].

Scanning Electron Microscopy (SEM)

The characterization was carried out at the Center for the Development of Advanced Materials and Nanotechnology of the National University of Engineering (UNI), as is known, the SEM (Hitachi Regulus model 8100) allows us to observe the morphology of the samples in the nanometric order and that it is of vital importance to observe how the particles of the ZnO film deposited on the electrode clump together. In all the samples, the wurtzite-type hexagonal structure of ZnO is observed (Figures 4 and 5).

Said figures also show the nanoporosity of the film. It is worth mentioning that for various percentages of Al_2O_3, it can be observed that said oxide is found in the film as shown in figures 6 and 7. The ZnO nanoparticles are shown in the form of rods with a hexagonal base of different sizes, both in the base and in their height, it is clearly observed that they are well-defined nanostructures.

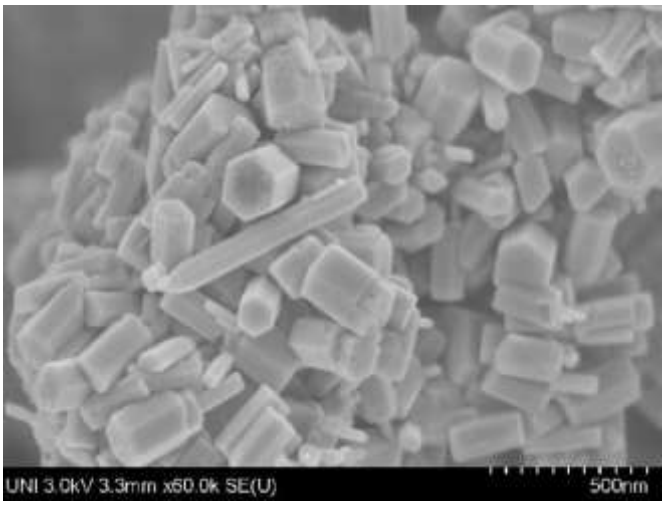

Fig. 4 SEM of ZnO (Wurtzite hexagonal structure).

The surface is a heterogeneous distribution and the crystallites are seen to have a size ranging from approximately 50 to 150 nm.

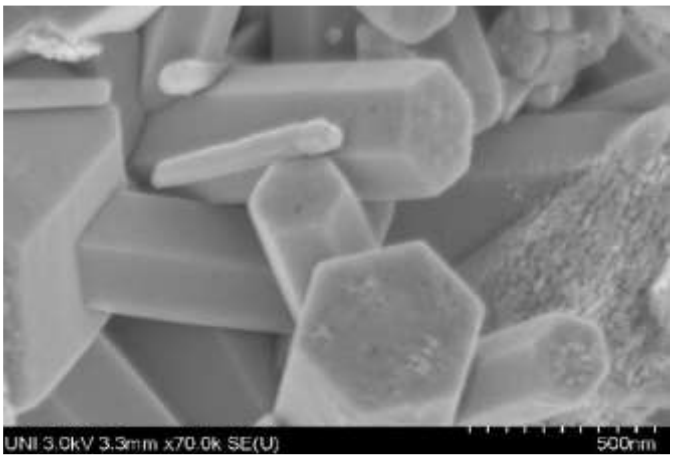

Fig.5 SEM of ZnO (Hexagonal Wurtzite Structure).

Figure 5 shows the individual ZnO crystals, it is worth mentioning, they are clearly visible, and their hexagonal grain base can be seen. The morphology and structure of the ZnO nanoparticles is determined by the concentration of TEA (triethanolamine), according to

publications, growth along the c axis is suppressed if we increase the concentration of TEA [17]. TEA forms complexes with Zn^{+2} and adsorbs on the ZnO surface, resulting in enhancement or inhibition of ZnO crystal growth along the different planes. In Figures 4, 5, 6 and 7 the crystallites have a hexagonal structure because the growth along the direction (0001) is greater than the direction $(01\bar{1}0)$.

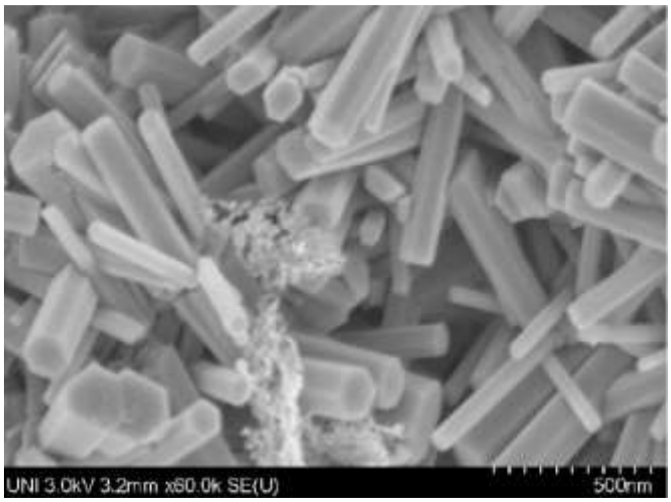

Fig. 6 SEM de ZnO con partículas de Al_2O_3 (1%)

Figure 6 shows an SEM image of a ZnO film modified with Al_2O_3 deposited on a conductive glass (SnO_2). Varying the percentages of Al_2O_3, the presence of flakes on the ZnO surface can be seen in the morphology of the electrode films.

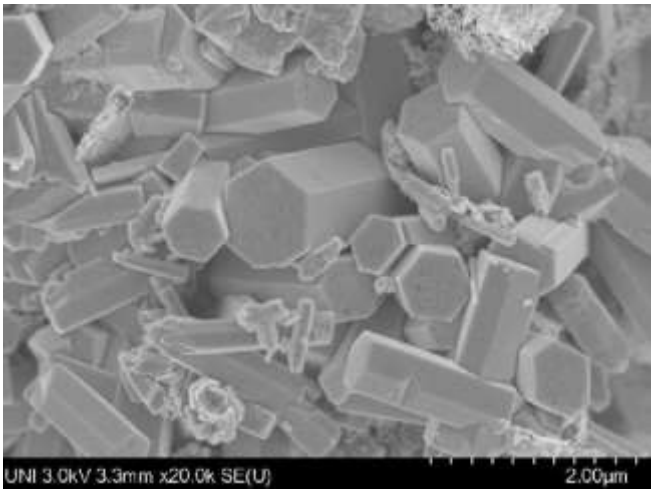

Fig.7. SEM of ZnO with Al_2O_3 nanoparticles (3%).

A slight increase in Al_2O_3 can be seen in Figure 7. The Al_2O_3 particles make the modified ZnO film denser than the unmodified films, and thus the specific surface area is increased, allowing a greater area of dye deposition.

Visible UV spectroscopy.

For this characterization, an Ocean Optics USB4000 brand spectrometer and an Ocean Optics brand DH2000 halogen light source were used. This technique allows us to determine the amount of light absorbed by the sample, it is very important that the absorption spectrum of the dye is in the visible (380-750 nm). Figure 8 shows that by means

of this UV-Vis spectroscopy technique it was possible to know the absorption wavelength that characterizes dye 719 is 530 nm, corroborating its photoactivity.

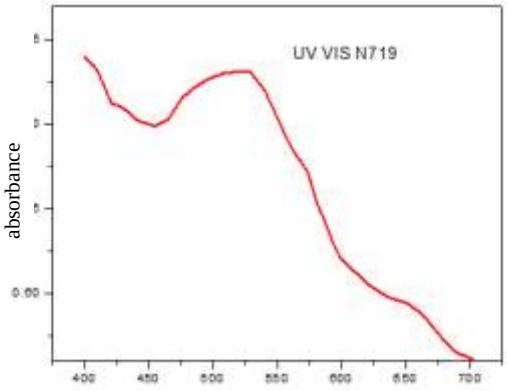

Fig. 8 Absorption spectrum of dye N719.

Figure 9 shows the modifications that occur in the absorption spectrum under different percentages of Al_2O_3.

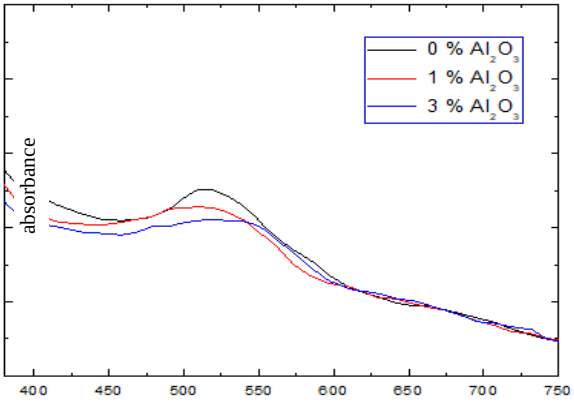

Fig. 9 Absorption spectrum of the ZnO electrode dye with different Al_2O_3 percentages.

Energy Dispersive Spectroscopy (EDS).

It can be seen in Figures 10, 11 and 12 that the EDS of the samples shows silicon and tin, which are elements of conductive glass (TCO). Since the electrode (ZnO) is modified with Al_2O_3 in minimal percentages, aluminum as an element will be appreciated in a minimal proportion (Figures 11 and 12).

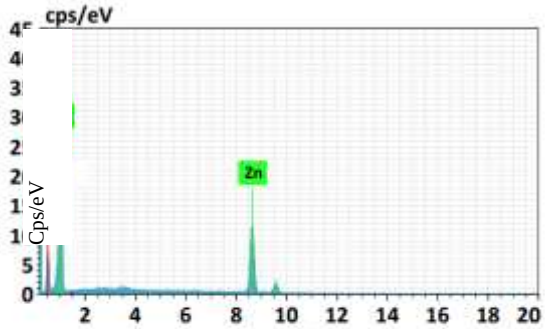

Fig. 10 EDS of the ZnO electrode (white).

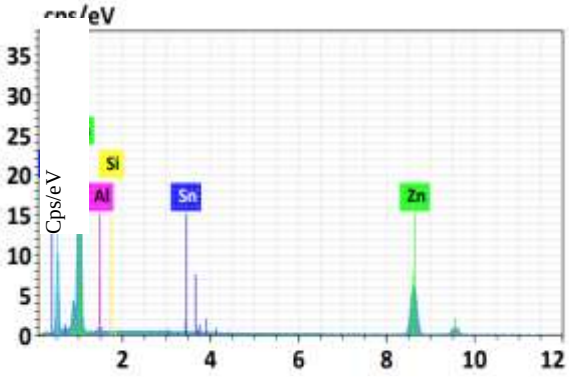

Fig. 11 EDS of the ZnO (1% Al2O3) electrode.

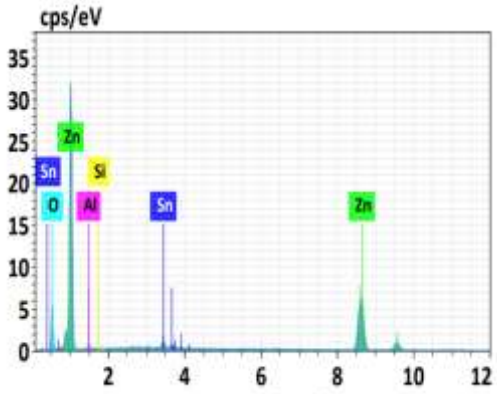

Fig. 12 EDS of the ZnO (3% Al2O3) electrode.

Characterization of the current-voltage (I-V) curve.

The I–V curve for ZnO-based dye-sensitized solar cells with the incorporation of different percentages of Al_2O_3, using $Al(NO_3)_3.9H_2O$ as precursor, are shown in Figures 13; 14 and 15 subjected to irradiation of 1000 W/m^2. These cells were stained with N719 in 0.5mM solution for 14 h. This characterization was carried out at the Center for the Development of Advanced Materials and Nanotechnology of the National University of Engineering, the equipment used is a Dyenamo Toolboox solar simulator. Said equipment shows the efficiencies with an error e=±0.001. The characterizations of the cells with different percentages of Al_2O_3 are shown below.

- **ZnO solar cell with 0% Al_2O_3**

In this case, the cell without modification shows an average efficiency of 0.330% (see Figure 13) with a short-circuit current density that varies from 1.02 to 1.15 mA/cm-2 and a circuit voltage variation open from 0.543 to 0.630 V, such data is shown in Table 2.

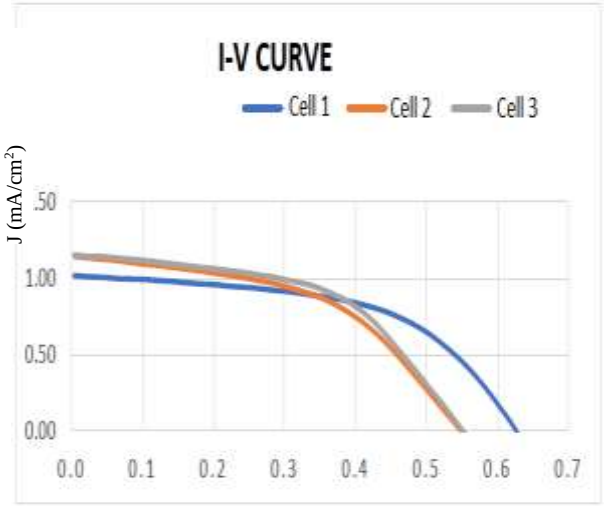

Voltage (V)

Fig. 13 I-V curve of three ZnO solar cells with 0% Al_2O_3.

Table 2. Efficiency of 3 ZnO solar cells with 0% Al2O3 ($\bar{n}$= 0.330; δ=0.013).

ZnO	η (efficiency) %	JSC (mA/cm^2)	V_{OC} (V)	FF
Cell 1	0.343	1,02	0,630	0,536
Cell 2	0.317	1,14	0,553	0,502
Cell 3	0.330	1,15	0,543	0,528

- **ZnO solar cell modified with 1% Al_2O_3**

When we modify the ZnO cell with 1% Al_2O_3, a relative improvement in average efficiency of 0.359% is achieved, which is due to the increase in current density (see Figure 14 and Table 3), that is, recombination of electrons is reduced.

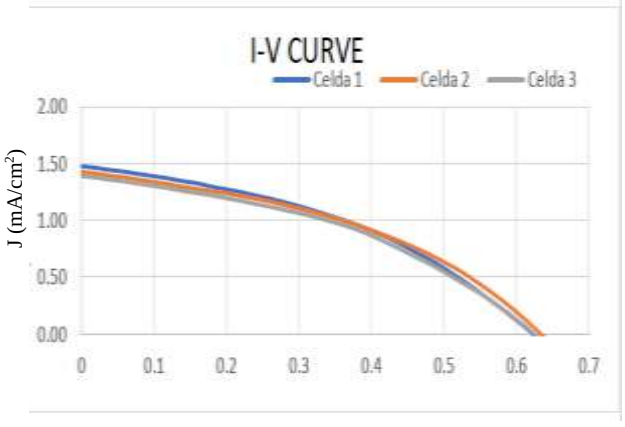

Voltage (V)

Fig. 14 I-V curve of three ZnO solar cells with 1% Al_2O_3.

Table 3. Efficiency of 3 ZnO solar cells with 1% Al_2O_3 ($\bar{n}$= 0.359; δ=0.006).

ZnO	η (efficiency) %	JSC (mA/cm^2)	V_{OC} (V)	FF
Cell 1	0,362	1,50	0,620	0,389
Cell 2	0,364	1,43	0,632	0,404
Cell 3	0,353	1,40	0,646	0,393

- **ZnO solar cell modified with 3% Al_2O_3.**

In this case, the ZnO cell modified with 3% Al_2O_3, the average efficiency is 0.392%, the open circuit voltages range from 0.620 to 0.646 V, and the current densities range from 1.40 to 1.50 mA/cm^2 (see Figure 15 and table 4).

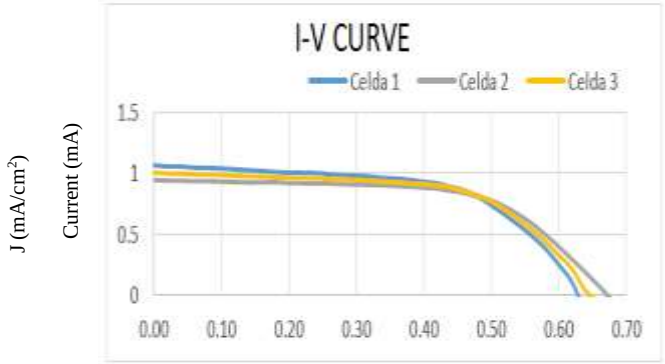

Fig. 15 I-V curve of three ZnO solar cells with 3% Al_2O_3.

Table 4. Efficiency of 3 ZnO solar cells with 3% Al_2O_3 ($\bar{n}$= 0.392; δ=0.003).

ZnO	η (efficiency) %	JSC (mA/cm^2)	V_{OC} (V)	FF
Cell 1	0,395	1,07	0,640	0,576
Cell 2	0,388	0,95	0,680	0,600
Cell 3	0,392	1,01	0,659	0,588

Table 5 shows the average efficiencies with their respective standard deviations of the cells with their Al_2O_3 percentages.

Table 5. Efficiencies of ZnO solar cells with different percentages of Al2O3.

% AL_2O_3.	η (efficiency) %	δ
0 %	0,330	0,013
1 %	0,359	0,006
2 %	0,392	0,003

Open Circuit Decay Voltage (OCVD)

It can be seen from figure 16 that when Al_2O_3 is added to the working electrode (ZnO) the voltages do not have slopes as steep as the blank ZnO.

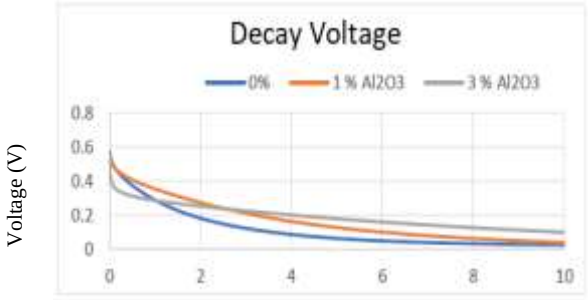

Fig. 16 Open circuit decay voltage with different Al_2O_3 percentages.

Photon to current conversion efficiency (IPCE).

The equipment used is a 300W Xenon-Ozone Free lamp coupled to a Cornerstone 260 monochromator (Oriel Quantum Efficiency Measurement Kit). From Figure 17 it can be seen that there is a maximum quantum efficiency at approximately 520nm, both in the unmodified and modified electrode. It is worth mentioning that the curves do not differ in their percentages of quantum efficiency.

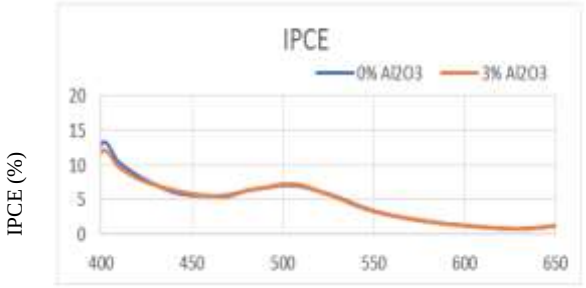

Fig. 17 IPCE of solar cells with various percentages of Al_2O_3.

Fourier Transform Infrared Spectroscopy (FTIR).

This characterization was carried out at the Center for the Development of Advanced Materials and Nanotechnology of the National University of Engineering, the equipment used is Thermo Fisher FTIR Spectrometers. With this characterization it is possible to determine the different chemical structures of the molecules, when IR radiation passes through a sample, said sample absorbs part of the radiation and the other part transmits it. Each chemical structure has its own spectral fingerprint. And through this characterization we can locate in the IR spectrum the OH groups whose assigned range is 3500-4000 cm^{-1}, as well as the carbonate groups (CO2 in the environment) as shown in figure 18. It is also necessary to mention that metallic oxides (M-O-M) are located in the 470 -1000 cm^{-1} band; ZnO is found in that band (526 cm^{-1}) as shown in figure 5.8; a small band is also shown at 710 cm^{-1} due to Al-O bonding. Regarding the functional groups of dye N719 as thiocyanate carboxylates, it is known that the thiocyanate ligand (-NCS) is found at 1728, 1610 and 1378 cm^{-1}.

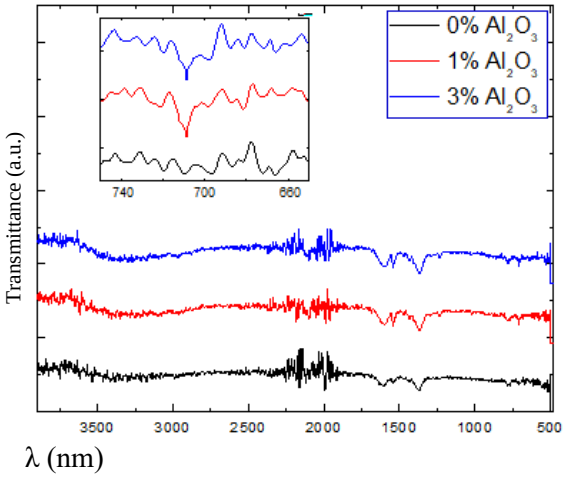

Fig. 18 FTIR of ZnO with various percentages of Al_2O_3.

Electrochemical Impedance Spectroscopy (EIS).

- **Data representation by Z view.**

The data obtained below was modeled using the Zview2 program (version 2.8d, Scribner Associates, Incel). This program provides us with the Nyquist diagram and the Bode diagram. The graphs of the impedances of 3 types of solar cells that differ according to the percentage of added Al_2O_3 with respect to the weight of ZnO are observed.

Figure 19 shows the impedance spectra of the cells, where it can be seen that they all consist of a semicircle (Nyquist diagram). Impedance as a function of frequency and phase offset as a function of frequency (Bode plot) are also shown.

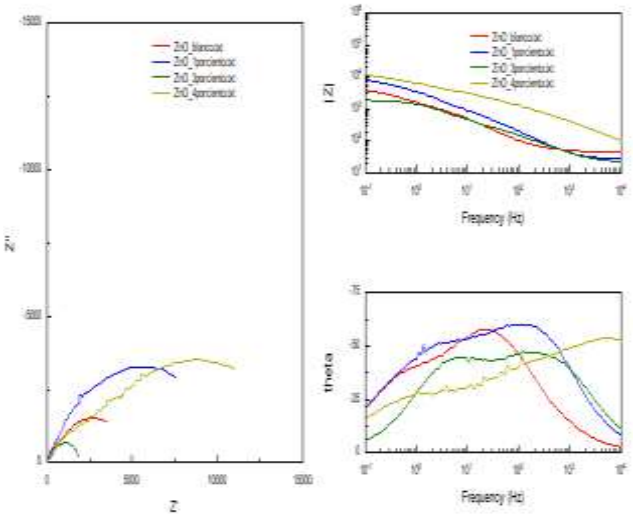

Fig. 19 Spectrum of the impedance of the solar cell (ZnO sensitized with N719) under a simulation of solar radiation (100 mW/cm^2) with different percentages of Al_2O_3: ZnO (red); 1% Al_2O_3 (blue); 3% Al_2O_3 (green) and 4% Al_2O_3 (yellow) accompanied by the impedance (Z) and the angle θ as a function of frequency.

In the following Figure 20 the spectra of the same solar cells have been obtained, but in the dark.

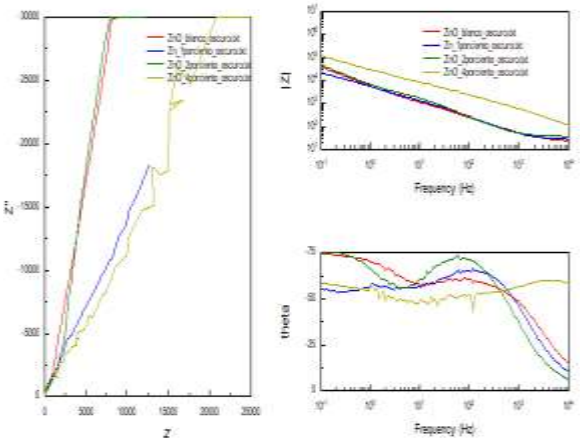

Fig. 20 Spectrum of the impedance of the solar cell (ZnO sensitized with N719) in the dark, with different percentages of Al2O3: ZnO (Red); 1% Al2O3 (Blue); 2% Al2O3 (Green) and 4% Al2O3 (yellow) accompanied by the graph of the impedance (Z) and the angle θ as a function of frequency.

It is necessary to mention that the data obtained in testing cells subjected to average potentials, is analyzed and adjusted by the Zview program. This program provides the values of the capacitor Cμ (CPE-T with its respective correction constant CPE-P, the which is known as the coefficient of ideality n). Therefore, the real capacitor, Cμ=CPE-T (jw)$^{CPE-P}$ [18].

As can be seen in Figures 21-23, there are two semicircles (Z1 and Z2) in all the cells and the third semicircle does not appear, that is, the impedance at low frequencies (Z3) is not observed, which corresponds to the Warburg element, corresponding to the diffusion of ions in the electrolyte.
The following shows the impedance graphs using the EIS:

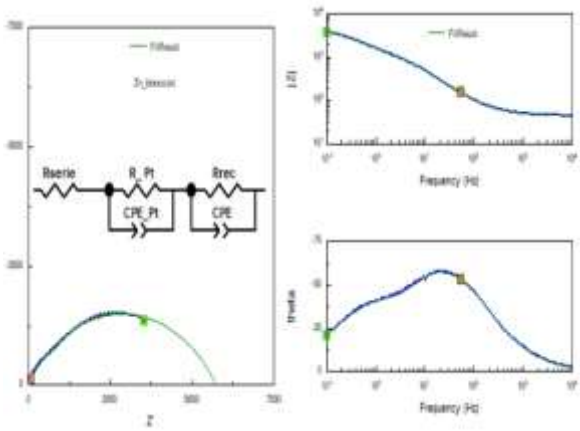

Fig. 21 Impedance spectrum of the ZnO solar cell (white) sensitized with N719, the data (blue) coincide with those provided by the Zview program settings (green).

In the modeled circuits of the ZnO-based solar cell, a series resistance called Rs is observed, which is represented in the graphs as the horizontal displacement of the spectrum with respect to the origin of coordinates.

The low frequency semicircle (Z1) is the result of the parallel association of the capacitance (C_{Pt}) with the charge transfer resistance in the platinized counter electrode.

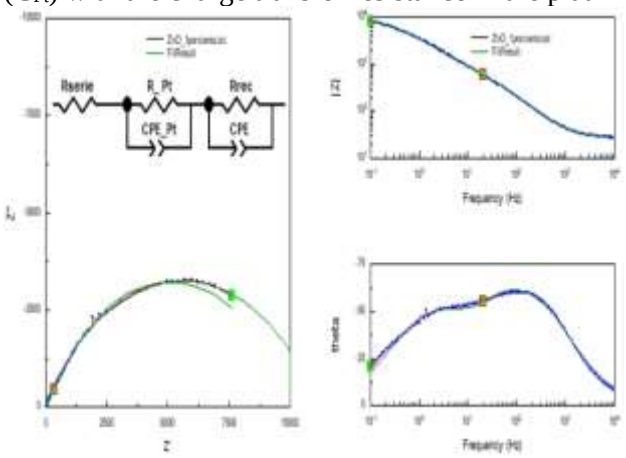

Fig. 22 Impedance spectrum of the ZnO solar cell with 1% Al2O3 sensitized with N719. Data obtained (red) and data adjusted by the Zview program (green).

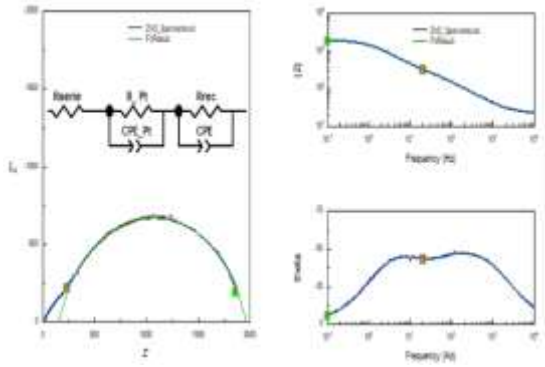

Fig. 23 Spectrum of the ZnO solar cell with 3% Al2O3 sensitized with N719. Data obtained (red) and data adjusted by the Zview program (green).

The Zview program provides us with approximate values of the elements of the internal impedance of the cells, such as Rtc (electrode resistance), Rrec (recombination resistance) and Cμ (electrochemical capacitance), which allows us to find the lifetime of the cell electron (τ_n) and transport time (τ_{trans}). The data found is shown in Table 6.

Table 6. Parameter results of ZnO-based solar cells sensitized with N719 dye with different weights of Al_2O3

% AL_2O_3	Rtr Ω	Rrec Ω	F Hz	Cμ μF	α	τ_n (ms)	τ_{trans} (ms)
0 %	150	371	0,23	53	0,71	19,6	7,9
1 %	195	305	0,21	56	0,75	17,0	10,9
2 %	145	371	0,19	61	0,71	22,6	8,8

Discussion

The ZnO solar cell modified with aluminum salt produces a better efficiency (n= 0.390%) when mixed with 3% Al_2O_3. And it also depends on the anion of the salt that was used, in this work Al $(NO_3)_3$ was used, it was tested with $AlCl_3$, but the results in efficiency were not as expected. The short circuit current also suffers a small increase from 1.02 to 1.07 mA when adding Al_2O_3. The open circuit voltage V_{OC} also had a small variation, from 0.63 to 0.65 V. The half-life of the electron (r_n) was also increased according to Table 5.6. It

can also be seen that when modified with 3% Al_2O_3 the r_n = 22.6 ms, achieving a small increase of 3ms with respect to the unmodified ZnO (r_n =19.6 ms) and this allows the electron to have more travel before recombination.

Conclusion

To conclude, ZnO was obtained at low temperatures through the sol-gel process, it was possible to improve the efficiency of the cell based on ZnO by incorporating Al_2O_3 (3%) to a maximum of 0.39%, achieving an improvement of 18% with respect to the unmodified ZnO solar cell. It is worth mentioning that a higher percentage increase of Al_2O_3 does not increase the efficiency of the cell, because in the impedance analysis it was noted that the resistance R_{rec} is reduced, producing recombination with the electrolyte and therefore a reduction in efficiency. On the other hand, in the electrochemical impedance analysis it was shown that the solar cell has a capacitive behavior like a capacitor presenting leaks. The recombination of the electron with the triiodide (ZnO/Dye/electrolyte interface) has the leakage behavior of a capacitor. In such analysis, to improve the cell efficiency, the resistance of the porous structure (R_{tc}) should always be less than the recombination resistance (R_{rec}) and also the resistance of the TCO (R_{TCO}) should be less than R_{rec}. It is important to mention that the degradation of the electrolyte negatively influences the performance of the cell. Regarding the morphological analysis of the electrode, it was possible to verify that the grains had the shape of a nanorod and that their sizes are determined by the concentrations of TEA (triethanolamine). The higher the concentration of TEA, the grain size is reduced and vice versa. Through the SEM it was determined that the size of the ZnO grains varies from 50 to 200 nm. It is also necessary to specify that the XRD did not directly detect the Al_2O_3 due to the minimum percentage that was added to the working electrode, however, with the EDS the aluminum element could be observed.

References

[1] Richard E. Smalley, “Future Global Energy Prosperity: The Terawatt Challenge,” MATERIAL MATTERS, vol. 30, Jun. 2005, [Online]. Available: www.mrs.org/publications/bulletin

[2] United Nations, “The milleniun development goals report.,” New York, 2015.

[3] J. Montero Amenedo, “TESIS DOCTORAL: Óxido de estaño dopado con antimonio y otros materiales relacionados con la conversión y ahorro de energía.,” UNIVERSIDAD COMPLUTENSE DE MADRID, Madrid, 2013.

[4] United Nations, “World Population Prospects 2019: Highlights,” New York, 2019.

[5] N. Asim et al., “A review on the role of materials science in solar cells,” Renewable and Sustainable Energy Reviews, vol. 16, no. 8. pp. 5834–5847, Oct. 2012. doi: 10.1016/j.rser.2012.06.004.

[6] A. Goetzberger and C. Hebling, “Photovoltaic materials, past, present, future,” Solar Energy Materials & Solar Cells, vol. 62, pp. 1–19, 2000.

[7] M. Gratzel, “Highly Efficient Nanocrystalline Photovoltaic Devices,” Platinum Metals Rev., pp. 151–159, 1994.

[8] Brian O’Regan & Michael Grätzel, “Bria"A low-cost, high-efficiency solar cell based on dyesensitized colloidal TiO2 films",” Nature, vol. 353, pp. 737–740, 1991.

[9] M. E. Quintana Cáceda, “Influencia del catalizador en la obtención de las fases cristalinas del óxido de titanio mediante el método del sol gel,” Tesis de maestría, Universidad Nacional de Ingeniería, Lima- Perú, 2004.

[10] María Esther Quintana Cáceda, “‘Celdas Solares de Óxido de Zinc Sensibilizadas con Colorante: Nuevos Enfoques’,” Tesis Doctoral, Universidad Nacional de Ingeniería, Lima – Perú, 2008.

[11] R. Nazario Ticse, “Celdas Grätzel de $TiO2$ sensibilizadas con el colorante natural Ayrampo (Opuntia Soehrensii), usando grafito como contraelectrodo.,” TESIS DE MAESTRIA, Universidad Nacional de Ingeniería , Lima, 2016.

[12] R. Nazario, W. S. Torres, E. Palacios, and M. Quintana, “Evaluación de capas de bloqueo en celdas solares sensibilizadas de óxido de titanio nanoestructurado,” Revista de la Sociedad Química del Perú, vol. 81, no. ISSN 1810-634X., pp. 109–121, 2015.
[13] K. Keis, L. Vayssieres, H. Rensmo, S.-E. Lindquist, and A. Hagfeldt, “Photoelectrochemical Properties of Nano- to Microstructured ZnO Electrodes,” J Electrochem Soc, vol. 148, no. 2, p. A149, 2001, doi: 10.1149/1.1342165.
[14] T. Ungár, “Microstructural parameters from X-ray diffraction peak broadening,” Scr Mater, vol. 51, no. 8 SPEC. ISS., pp. 777–781, 2004, doi: 10.1016/j.scriptamat.2004.05.007.
[15] Y. Gao, M. Nagai, T. C. Chang, and J. J. Shyue, “Solution-derived ZnO nanowire array film as photoelectrode in dye-sensitized solar cells,” Cryst Growth Des, vol. 7, no. 12, pp. 2467–2471, Dec. 2007, doi: 10.1021/cg060934k.
[16] P. Basnet, D. Samanta, T. Inakhunbi Chanu, J. Mukherjee, and S. Chatterjee, “Assessment of synthesis approaches for tuning the photocatalytic property of ZnO nanoparticles,” SN Appl Sci, vol. 1, no. 6, Jun. 2019, doi: 10.1007/s42452-019-0642-x.
[17] M. A. Haque and S. Mahalakshmi, “Effect of Triethanolamine on Zinc Oxide Nanoparticles,” Materials Focus, vol. 2, no. 6, pp. 469–474, Dec. 2013, doi: 10.1166/mat.2013.1117.
[18] S. Zheng, Q. Fang, and I. Cosic, “An investigation on dielectric properties of major constituents of grape must using electrochemical impedance spectroscopy,” European Food Research and Technology, vol. 229, no. 6, pp. 887–897, 2009, doi: 10.1007/s00217-009-1126-9.